Geophysical Research Letters

RESEARCH LETTER
10.1029/2018GL078327

Key Points:
- Relationships between a diverse array of lunar mare effusive and explosive volcanic deposits and landforms have previously been poorly understood
- Four phases in the generation, ascent, and eruption of magma and gas release patterns are identified and characterized
- Specific effusive, explosive volcanic deposits, and landforms are linked to these four phases in lunar mare basalt eruptions in a predictive and integrated manner

Correspondence to:
J. W. Head,
james_head@brown.edu

Citation:
Wilson, L., & Head, J. W. (2018). Controls on lunar basaltic volcanic eruption structure and morphology: Gas release patterns in sequential eruption phases. *Geophysical Research Letters*, *45*, 5852–5859. https://doi.org/10.1029/2018GL078327

Received 11 APR 2018
Accepted 1 JUN 2018
Accepted article online 7 JUN 2018
Published online 20 JUN 2018

Controls on Lunar Basaltic Volcanic Eruption Structure and Morphology: Gas Release Patterns in Sequential Eruption Phases

L. Wilson[1,2] and J. W. Head[2]

[1]Lancaster Environment Centre, Lancaster University, Lancaster, UK, [2]Department of Earth, Environmental and Planetary Sciences, Brown University, Providence, RI, USA

Abstract Assessment of mare basalt gas release patterns during individual eruptions provides the basis for predicting the effect of vesiculation processes on the structure and morphology of associated features. We subdivide typical lunar eruptions into four phases: *Phase 1*, dike penetrates to the surface, transient gas release phase; *Phase 2*, dike base still rising, high-flux hawaiian eruptive phase; *Phase 3*, dike equilibration, lower flux hawaiian to strombolian transition phase; and *Phase 4*, dike closing, strombolian vesicular flow phase. We show how these four phases of mare basalt volatile release, together with total dike volumes, initial magma volatile content, vent configuration, and magma discharge rate, can help relate the wide range of apparently disparate lunar volcanic features (pyroclastic mantles, small shield volcanoes, compound flow fields, sinuous rilles, long lava flows, pyroclastic cones, summit pit craters, irregular mare patches, and ring moat dome structures) to a common set of eruption processes.

Plain Language Summary Since the early days of close-up orbital observations of the lunar surface in the 1960s, a large number of lunar volcanic landforms have been identified and cataloged, including explosive volcanic mantles, small shield-shaped volcanoes, compound flow fields, meandering sinuous rille channels, long lava flows, volcanic cones, volcanic pit craters, and very unusual and enigmatic features called irregular mare patches and ring moat dome structures. Unknown is how all of these different features form and how they might fit together in different stages or phases of lunar volcanic eruptions. Interpretation is complicated by the effects of low lunar gravity and lack of an atmosphere, both encouraging very different patterns of gas release during lunar volcanic eruptions. We examine the nature of the rise, eruption, and gas release of lavas from the lunar interior and show how four phases of mare basalt eruptions can help relate the wide range of apparently disparate lunar volcanic features to a common set of eruption processes. This is important because it links the observed geologic record to specific physical volcanology predictions that can be further tested with future exploration and analysis.

1. Introduction

Beginning with the acquisition of high-resolution images of the lunar surface from orbit, a very wide and diverse array of morphologic features has been observed in association with the lunar maria (e.g., flows, domes, cones, graben, sinuous rilles, ridges, pits, dark halo, and mantle deposits; Schultz, 1976; Wilhelms, 1987). Unclear has been the interpretation of each of these features and how they might relate to specific eruption conditions and the range of eruptions styles. We synthesize recent developments in understanding the origins and volatile contents of lunar magmas, the mechanisms that transferred magma to the surface, and the factors that controlled the eruption style of the resulting volcanism with emphasis on the effects of volatile formation and release. We show how the specific influences of the physical environment, especially the small value of the acceleration due to gravity and the negligible atmospheric pressure, serve to combine with the nature and mode of volatile behavior to produce the observed spectrum of lunar surface volcanic features.

2. Constraints on Lunar Magmatism

Lack of evidence for crustal contamination in lunar lava samples implies that most lunar eruptions involved basaltic magma that passed rapidly from its mantle source to the surface (Shearer et al., 2006). A model that readily explains this involves dikes nucleating at the tops of ~500-km-deep mantle partial melt zones (diapirs)

when the slowly convectively rising diapirs encountered host rocks cool enough that the combination of host viscosity and diapir-imposed strain rate exceeded the ability of the host rocks to deform plastically, so that a brittle fracture nucleated (Wilson & Head, 2017a). Seepage of buoyant melt into the resulting crack caused the slow (decades?) growth of a dike that when a critical length of at least several tens of km was reached, disconnected from the diapir source and migrated rapidly upward (a few hours) through the mantle above it. The dike would have penetrated the low-density lunar crust to an extent determined by the balance between the positive buoyancy of its lower part still in the mantle and the negative buoyancy of it upper part in the crust. A few dikes penetrate to a shallow low-density impact crater-related crustal zone and produce crater-contained sills known as floor-fractured craters (Jozwiak et al., 2012; Jozwiak et al., 2015) with consequent evolution of the intruded magma (Wilson & Head, 2018). A sufficiently vertically extensive dike completely penetrating the crust would break through to erupt at the surface. The great vertical extent of the dike meant that the major lunar magmatic volatile, CO, was produced in amounts up to at least 1,000 ppm by mass over a wide range of depths in the dike, potentially extending down to at least 50 km in a large enough dike. Additionally, up to at least 1,000 ppm of water and sulfur compounds were released in the upper few hundred meters of dikes (Rutherford et al., 2017). We explore the effects of this behavior in the lunar environment.

3. Distinctive Characteristics of Lunar Volcanism

The absence of an appreciable atmospheric pressure caused basaltic volcanic eruptions on the Moon to have a vigorously explosive nature, despite the low magmatic volatile content by Earth standards. This was especially true at the start of an eruption due to concentration of volatiles into the upper parts of dikes approaching the surface (Wilson & Head, 2003). However, the lunar versions of hawaiian and strombolian explosive activities differed greatly from those on Earth (Wilson & Head, 1981), with no lunar analog of a convecting Plinian eruption cloud (Head & Wilson, 2017). The extreme expansion of even the smallest gas bubbles disrupted magma into pyroclasts predominantly submillimeter in size. These clasts were accelerated by the expansion of the released gases until the gas pressure became so low that the Knudsen regime was reached and the interactions between gas and clasts became negligible; the clasts then continued on ballistic trajectories until they reached the surface.

The giant 50- to 90-km-long, 30- to 100-m-wide dikes transferring magma volumes of up to ~1,000 km^3 to the lunar surface rose from the mantle at speeds of tens of m/s, and initially delivered magma volume fluxes of up to ~10^6 m^3/s through the vents that they created to feed hawaiian-style lava fountains (Wilson & Head, 2017a). The combination of high volume flux and small pyroclast size caused many lunar lava fountains to be very optically dense, especially those with relatively low volatile contents. Pyroclasts in the hot cores of such fountains were unable to radiate heat into space and thus landed at magmatic temperature to coalesce into several hundred kilometer-long lava flows that, having lost almost all of their gas, were nearly completely vesicle-free. This condition continued as the rising dike decelerated toward buoyancy equilibrium and the erupted volume flux decreased to ~10^5 m^3/s. Once buoyancy equilibrium was achieved, the erupted flux would have decreased to ~10^4 m^3/s as dike closure driven by lithospheric stresses dominated the activity. Only when the volume flux decreased to less than ~3×10^4 m^3/s would the lava fountain have begun to be optically transparent allowing extensive pyroclast cooling. Long-lived eruptions of relatively volatile-poor magmas at these intermediate volume fluxes were responsible for the thermo-mechanical erosion of the characteristic lunar sinuous rille channels (Hurwitz et al., 2012). The relative duration of activity, and hence magma volumes erupted, at these varying volume fluxes was a function of the vertical extent of the dike relative to the thickness of the lunar crust. Figure 1 gives typical values.

Many lunar magmas appear to have released a few hundred ppm of mainly CO as they erupted. In contrast, total magma volatile mass fractions of up to 3,000 ppm (Rutherford et al., 2017) in some picritic magmas led to pyroclast speeds in steady eruptions of up to 220 m/s and maximum ranges of ~30 km. Greater speeds and ranges were possible in the initial stages of eruptions as gas concentrated in the upper tips of dikes was released, and the combination of these conditions produced extensive regional pyroclastic blankets (Head & Wilson, 2017).

Since all eruptions began with the arrival of a dike at the surface, initial vents were always explosively erupting fissures, generally with lengths up to ~15 km (Head & Wilson, 2017). If the fissure length was much less

Eruption Phase	PHASE 1	PHASE 2	PHASE 3	PHASE 4
	Dike penetrates to surface, transient gas release phase	Dike base still rising, high flux hawaiian eruptive phase	Dike equilibration, lower flux hawaiian to strombolian transition phase	Dike closing, strombolian vesicular flow phase
Dike Configuration	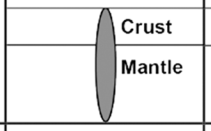	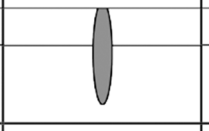	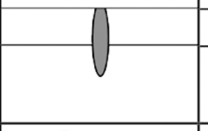	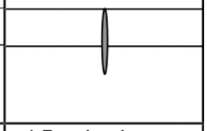
Surface Eruption Style	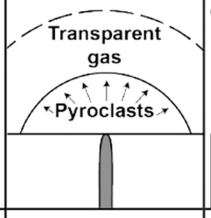	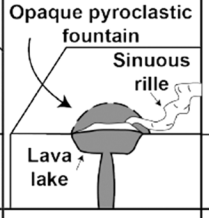	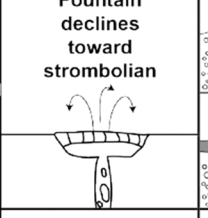	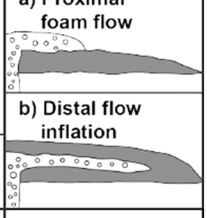
Magma Rise Speed	30 to 20 m/s	20 to 10 m/s	5 to <1 m/s	< 1 m/s
Magma Volume Flux	~10^6 m^3/s	10^6 to 10^5 m^3/s	10^5 to ~10^4 m^3/s	~10^4 m^3/s
Percent Dike Volume Erupted	<5%	~30%	~30%	~35%
Phase Duration	~3 minutes	5-10 days	2-3 days	10-100 days
Flow Advance Rate	n/a	~3 to 0.1 m/s	0.03 m/s	0.01 m/s
Flow Advance Distance	n/a	300 km	305 km	335 km
Vesicularity of Flow	n/a	zero	low, but increasing	very high

Figure 1. The characteristics of the four eruption phases during a typical lunar eruption, with diagrams and parameters representing average values. The relative duration of individual phases depends on the total dike volume and vertical extent.

than the maximum range of the pyroclasts, gas effectively expanded radially from a point source, producing a circular, umbrella-shaped fire fountain like those seen on Io (Wilson & Head, 2001), though of very much smaller size (Head et al., 2002) due to the much smaller volatile contents of the lunar magmas (Head & Wilson, 2017). If the fissure length was comparable to or greater than the maximum pyroclast range, the fissure acted as a line source and gas mainly expanded sideways away from the fissure, not radially. These differing patterns of gas expansion and clast dispersal cause a concentration of clasts in the outer edges of elongate fountains, enhancing their optically density. On the basis of these principles, we now examine the stages in the evolution of a typical lunar mare basalt eruption to assess predictions for resulting structures, landforms, and volatile fate.

4. Evolution of a Typical Lunar Basaltic Eruption: The Four Phases

In order to link the ascent and eruption of magma to the observed landforms and structures, we identify four phases in the evolution of a typical lunar eruption and examine how variations in dike total volume, magma flux, gas content, and eruption duration during each phase produce different landforms (Figure 1).

Phase 1. (Dike penetrates to surface, transient gas release phase) is very explosive due to volatile concentration into the low-pressure region near the upper tip of the propagating dike, but is short-lived (Wilson & Head, 2003). In the extreme tip of the dike a zone of pure gas may extend for 100–200 m, below which will be a foam layer with a high vesicularity extending downward for ~10 km. Complete eruption of this gas-rich magma would have taken as little as 3 min and produced a very widespread but extremely thin deposit (Head & Wilson, 2017), consistent with the ubiquitous volcanic glass beads found in soils even in the highlands.

Phase 2. (Dike base still rising, high flux hawaiian eruptive phase), during which the dike as a whole is still rising toward a neutral buoyancy configuration, has the highest magma discharge rate ~10^6 m^3/s, and involves the near-steady explosive eruption of magma with a volatile content representative of the bulk of the magma. This would have involved the formation of a relatively steady, largely optically dense hawaiian fire fountain within which submillimeter-sized pyroclastic droplets would have lost gas efficiently and accumulated with negligible cooling within a few to 10 km of the fissure to form a vesicle-deficient lava lake. Lava would have flowed away from the lake in an initially turbulent manner to form the distal part of the eventual lava flow deposit in the case of a short-lived eruption, or to feed a flow eroding a sinuous rille in the case of a sufficiently long-lasting eruption (Figure 1). Given the relative vertical extents of typical mantle dikes, ~50–90 km (Wilson & Head, 2017a), and the thickness of the lunar crust (~30 km; Wieczorek et al., 2013), a significant part of the total dike magma volume would have been erupted during this phase. Typically, the duration of this phase would have been ~5–10 days, with erupted magma volume fluxes decreasing from ~10^6 to ~10^5 m^3 s^{-1} during this period.

Phase 3. (Dike equilibration, lower flux hawaiian to strombolian transition phase) begins when the dike feeding the eruption approaches an equilibrium, with the positive buoyancy of its lower part in the mantle balancing the negative buoyancy of its upper part in the crust (Figure 1). The lower dike tip then stops rising, and the dike's vertical extent becomes fixed. The main process driving this phase of the eruption is now the horizontal reduction in the thickness of the dike as both its internal excess pressure and the forced deformation of the host rocks by the intrusion of the dike relax (Wilson & Head, 2017a). While deformation of host rocks in the shallow crust is probably elastic and rapid, deformation of hotter mantle rocks surrounding the lower part of the dike is visco-elastic or viscous, resulting in a much longer time scale. During this period, the vertical rise speed of the magma in the dike decreases greatly to less than 1 m/s, implying that the magma volume flux leaving the vent similarly decreases to a few ×10^4 m^3/s over the course of two to three days. The reduced vertical magma flow speed means that gas bubbles nucleating throughout the vertical extent of the dike can now rise at an appreciable rate through the liquid, and there is time for larger bubbles, especially the CO bubbles being produced at great depths, to overtake smaller bubbles leading to coalescence and even greater growth. This leads to very large bubbles—gas slugs—filling almost all of the width of the dike and producing strombolian explosions at the surface (Parfitt & Wilson, 1995). The change from hawaiian to strombolian activity occurs quickly.

Phase 4. (Dike closing, strombolian vesicular flow phase) begins when the activity has become entirely strombolian. Tectonic stresses continue to cause horizontal dike closure and magma extrusion at a low flux. Magma from the deepest parts of the dike is still being forced upward to lower pressure levels and so is continuing to produce some CO at all depths, and very minor strombolian explosive activity continues above the vent as a result. However, a stable crust forms on the magma still emerging from the vent and flowing away as lava.

There are two important potential consequences of Phase 4 activity. In some cases (Phase 4a, low flux), this phase might begin only after most of the magma in the dike has already been erupted and the volume flux has decreased to a very low level (Figure 1). This would be the case for a dike that had a relatively small vertical extent, so that most of its magma was erupted while the dike was still achieving equilibrium. The most likely consequence is then the emplacement in the vicinity of the vent of vesicular lava as a series of cooling-limited flows superimposed on earlier eruption products, in some cases building a small, low shield around the vent. The magma being erupted now consists of liquid containing bubbles of a mixture of gases and volatile elements (Gaillard & Scaillet, 2014; Renggli et al., 2017; Saal et al., 2018) defined by the thermodynamic equilibrium between the products of interactions between mainly H_2O and sulfur species released over

the last <500 m of magma rise (Rutherford et al., 2017). These bubbles would have nucleated with diameters of ~10–20 μm and would have grown to ~20–30 μm at the surface, remaining stable within the body of the lava as surface tension forces (Wilson & Head, 2017b) imposed a retaining pressure of ~30 kPa. Lunar basalts exsolving ~1,000 ppm of these gases would have left the fissure vent as lava foams with vesicularities of more than 90% by volume. Radiative cooling of the surface would have aided the stabilization of the bubbles at the top surface of the foam, but would also have induced differential cooling stresses, and it is likely that the topmost bubbles would have exploded into the overlying vacuum producing a layer of bubble wall shards with sizes of ~10 μm. As long as gas could escape easily through this accumulating debris layer, a wave of foam disintegration would have propagated downward through the foam, increasing the thickness of the layer. However, this wave would rapidly have reached depths where there had been no cooling, and so the disrupted bubble wall fragments would have formed droplets that would have welded with one another, forming a less vesicular layer with some finite strength which, aided by the weight of the accumulated debris above, would have inhibited further foam disintegration.

The weight of the overlying material would have determined the local pressure as a function of depth and hence the depth down to which volatile exsolution could occur. The pressure at 1 m depth in vesicular lava on Earth is typically 115 kPa, whereas at that depth on the Moon the value is ~1 kPa, 100 times less. In general, therefore, Phase 4a low flux lava flows would have consisted of a fragmental layer overlying a very vesicular layer. Collapse of such flows could be consistent with the morphology of some of the irregular mare patches (IMPs) documented by Braden et al. (2014) in the maria. If the flows are thick enough, these vesicular layers could, in turn, overlie a layer of lava still containing dissolved volatiles. This as-yet unvesiculated layer would become important as the lava cooled and crystallized if volatile concentration into the remaining liquid caused second boiling and additional postemplacement vesiculation.

In other cases, with vertically more extensive dikes (Phase 4b, high flux), this phase might commence with a large fraction of the total dike magma still being available for extrusion as vesicular lava. In such cases this lava is likely to intrude into the still-hot interiors of the previously emplaced nonvesicular flows and cause them to inflate. A similar pattern of late-stage magma intruding earlier-emplaced flow lobes is documented for flood-basalt lava fields on Earth (Self et al., 1996). In the lunar case, the lower parts (<400 m depth) of the dike feeding such intruding flows would contain water and sulfur compounds that had not yet been exsolved. On a timescale of weeks, the resulting compound flows would cool, and the concentration of volatiles into the residual liquid as crystallization occurred would lead to second boiling, with the resulting new population of gas bubbles causing a further, possibly extensive, inflation episode. Extrusion of the resulting magmatic foam through cracks in the lava crust may be an explanation of the ring moat dome structures (RMDSs; Zhang et al., 2017) found in large numbers on many mare flows.

The total duration of Phase 4 of an eruption would have been controlled by the nature and magnitude of the global stress state of the lithosphere, influencing visco-elastic relaxation of the host rocks, and by cooling of the magma in the dike. Lunar thermal history (Solomon & Head, 1980) suggests that the lithosphere was under extensional stresses for the first ~1 Ga as radiogenic heat accumulated and fed the onset of mare volcanism, followed at about 3.6 Ga by compressive stresses as the interior cooled, encouraging faster closure of dikes in geologically more recent eruptions. Dike models (Wilson & Head, 2017a) suggest that Phase 4 dikes would have had initial widths of at least 10–20 m, and cooling of near-stagnant magma in such dikes by conduction alone would require one to two years following the end of the eruption.

5. Posteruption Changes in Flows

After the main phases of an eruption are complete and all motion has ceased, changes still occur. Cooling of lava takes place at all boundaries, causing contractional stresses in the thickening surface crust. Lava shrinks as its density increases, causing subsidence which is greatest where lava has infilled preeruption depressions, thus adding differential stresses. These can combine to form fractures in the cooled crust. Crystallization due to cooling increases the concentration of residual volatiles in the remaining magmatic liquid causing supersaturation, and second boiling leads to additional gas bubble nucleation. Where supersaturation and second boiling occur in regions of a flow that already contain a foam core, expansion of the foam and extrusion of foam through cracks onto the lava flow surface can occur.

6. Consequences for Observed Volcanic Features

The volcanic features formed during these various phases of activity would have depended critically on the vent configuration and the magma discharge rate and volatile content during the various stages of the eruption. We identify nine different features typical of lunar volcanic eruptions (Head & Wilson, 2017) and link them to the four eruptive phases described above.

1. *Pyroclastic mantles* form as the gas-rich tip of a dike initially reaches the surface and can represent the products of Phase 1. All lunar eruptions should include such a phase, though the deposit may be very thin and easily masked by regolith formation or subsequent volcanic activity in low to moderate volatile content magmas. Additional pyroclasts can be dispersed around the vent for hundreds of meters to several tens of kilometers as magmatic volatile content varies during Phase 2 hawaiian eruptions.
2. *Small shield volcanoes* consist of Phase 2 lavas erupted from dikes that have a relatively small volume, so that neither the erupted volume nor the volume flux are large. Overflows from the lava lake around the vent are fed at a low eruption volume flux and the resulting lava flows do not travel far (~5–15 km) before stopping due to cooling. Previous flow deposits form obstacles to subsequent lava outflows from the pond and so eventually flows will have left the pond in all radial directions and a low shield volcano progressively accumulates. Subsequent Phase 3/4 activity builds additional features at the summit of the volcano (strombolian spatter and foam layers). Phase 4 (a) activity could also result in small, low shield volcanoes with superposed foam layers and IMPs, such as Cauchy 5 (Qiao et al., 2018).
3. *Compound flow fields* (Kreslavsky et al., 2017) form from relatively small-volume dikes with low eruption fluxes. In contrast to small shield volcanoes that would form at central vents on very low slopes, compound flow fields form from fissure eruptions on appreciable slopes. Cooling limited flows induce multiple marginal breakouts upslope toward the vent, producing the digitate map outline typical of compound flow fields.
4. *Sinuous rilles and their source depressions* are initiated during Phase 2 eruptions from dikes containing a large volume of low volatile content magma that erupts through a fissure less than ~5 km long, ensuring a moderate volume flux. This generally creates a near-circular lava pond that contains lava at magmatic temperature fed from an optically dense lava fountain. The pond feeds a turbulent lava flow that efficiently erodes its substrate to form a sinuous channel over the course of a few months as the eruption continues through Phases 3 and 4.
5. *Long lava flows* represent Phase 2 eruptions from large-volume dikes that feed fissure vents 10–15 km long. The magma volatile content has little influence on the morphology of the distal parts of the flow field emplaced from the early stages of the eruption because the high magma volume flux guarantees an optically dense fire fountain forming a lava lake at magmatic temperature, in turn feeding hot, turbulent volatile-free lava flows. However, the magma volatile content becomes important later in Phases 3 and 4.
6. *Pyroclastic cones* form during Phases 3 and 4 of eruptions with an intermediate volatile content. The change from steady to pulsating hawaiian activity, as the eruption progresses toward the strombolian stage, allows the outer parts of the fire fountain to become partially transparent so that partially cooled pyroclasts reach the ground to form spatter or cinder cones, the degree of welding depending on the precise amount of cooling.
7. *Summit pit craters* can initially form from Phase 2 pyroclastic activity in low effusion rate, small-shield building eruptions, with hawaiian pyroclast ranges out to ~0.5–1.5 km radius. They may also be the result of Phase 4a activity from small-volume dikes erupting volatile-poor magma from small shield summit vents, coupled with volume adjustments during late-stage magma cooling. They also appear to commonly involve only short fissure vents, so that although the low volatile content causes short pyroclast ranges, nevertheless, a small and roughly circular lava pond forms around the vent. In one case (Hyginus), escape of gas that has accumulated in lateral dikes linked to the summit vent created a caldera (Wilson et al., 2011).
8. *IMPs* are interpreted to be related to Phase 4a activity from small-volume dikes. After explosive activity becomes minimal, very vesicular magma from the dike is emplaced under a cooling crust on the lava lake around the vent. In some cases this magmatic foam breaks through the crust to form bulbous mounds that represent one class of IMP, as at the small shield summit crater Ina (Qiao et al., 2017). In other cases the foam intrusion raises the crust of the crater lake and overflows onto the upper flanks, where partial

collapse of the foam produces another type of IMP, such as those on the flanks of Cauchy 5 (Qiao et al., 2018). Similar features occur on the floor of the Hyginus collapse caldera (Braden et al., 2014).

9. *RMDSs* (Zhang et al., 2017) are interpreted to be the consequence of Phase 4b activity from a large-volume dike. Earlier phases of the eruption emplace long volatile-free lava flows. The Phase 4b activity injects partly vesiculated lava into the hot cores of the earlier flows causing inflation. Subsequent cooling and crystallization drive exsolution of the remaining volatiles (second boiling), causing even more inflation and producing large amounts of magmatic foam. Escape of the foam through cracks in the cooled crust of the flow forms RMDSs. The moat surrounding the low dome structure is interpreted to represent the consequence of the loading due to the extruded material coupled with conservation of volume as the extrusion occurs.

7. Conclusions

We have used the basic principles of magma generation, ascent, and eruption to examine the range of dike volumes, effusion rates, volatile species, and release patterns as a function of time and eruption duration, subdividing eruptions into four sequential phases with specific individual characteristics and predictions. These phases result in a unifying quantitative conceptual model for the relationships among a wide and diverse range of related observed volcanic landforms and structures such as pyroclastic mantles, small shield volcanoes, compound flow fields, sinuous rilles and their source depressions, long lava flows, pyroclastic cones, summit pit craters, IMPs, and RMDSs. In contrast to viewing the array of volcanic landforms each in isolation, these theoretical predictions provide the basis for placing lunar volcanic landforms into eruptive sequences from individual eruptive events, and linking them to potential variations in dike characteristics and evolution, effusion rates, and volatile contents, that can provide clues to the nature of magma source regions. These predictions and correlations can be further tested by future human and robotic lunar exploration to specific destinations.

Acknowledgments

L. W. thanks the Leverhulme Trust for support through an Emeritus Fellowship. We gratefully acknowledge funding to co-investigator J. W. H. for participation in the LOLA Experiment Team (grants NNX11AK29G and NNX13AO77G from the National Aeronautics and Space Administration - Goddard). Much of the synthesis work for this contribution was enabled by participation in the NASA Solar System Exploration Research Virtual Institute, through the SEEED (SSERVI Evolution and Environment of Exploration Destinations) cooperative agreement number NNA14AB01A at Brown University. Thanks are extended to Anne Côté for help in figure drafting and preparation. We thank an anonymous reviewer for useful comments. No new data were used in producing this manuscript.

References

Braden, S. E., Stopar, J. D., Robinson, M. S., Lawrence, S. J., van der Bogert, C. H., & Hiesinger, H. (2014). Evidence for basaltic volcanism on the Moon within the past 100 million years. *Nature Geoscience*, *7*(11), 787–791. https://doi.org/10.1038/NGEO2252

Gaillard, F., & Scaillet, B. (2014). A theoretical framework for volcanic degassing chemistry in a comparative planetology perspective and implications for planetary atmospheres. *Earth and Planetary Science Letters*, *403*, 307–316. https://doi.org/10.1016/j.epsl.2014.07.009

Head, J. W., & Wilson, L. (2017). Generation, ascent and eruption of magma on the Moon: New insights into source depths, magma supply, intrusions and effusive/explosive eruptions (Part 2: Observations). *Icarus*, *283*, 176–223. https://doi.org/10.1016/j.icarus.2016.05.031

Head, J. W., Wilson, L., & Weitz, C. M. (2002). Dark ring in southwestern Orientale basin: Origin as a single pyroclastic eruption. *Journal of Geophysical Research*, *107*(E1), 5001. https://doi.org/10.1029/2000JE001438

Hurwitz, D. M., Head, J. W., Wilson, L., & Hiesinger, H. (2012). Origin of lunar sinuous rilles: modeling effects of gravity, surface slope, and lava composition on erosion rates during the formation of Rima Prinz. *Journal of Geophysical Research*, *117*, E00H14. https://doi.org/10.1029/2011JE004000

Jozwiak, L. M., Head, J. W., & Wilson, L. (2015). Lunar floor-fractured craters as magmatic intrusions: Geometry, modes of emplacement, associated tectonic and volcanic features, and implications for gravity anomalies. *Icarus*, *248*, 424–447. https://doi.org/10.1016/j.icarus.2014.10.052

Jozwiak, L. M., Head, J. W., Zuber, M. T., Smith, D. E., & Neumann, G. A. (2012). Lunar floor-fractured craters: Classification, distribution, origin and implications for magmatism and shallow crustal structure. *Journal of Geophysical Research*, *117*, E11005. https://doi.org/10.1029/2012JE004134

Kreslavsky, M. A., Head, J. W., Neumann, G. A., ZUber, M. T., & Smith, D. E. (2017). Low-amplitude topographic features and textures on the Moon: Initial results from detrended Lunar Orbiter Laser Altimeter (LOLA) topography. *Icarus*, *283*, 138–145. https://doi.org/10.1016/j.icarus.2016.07.017

Parfitt, E. A., & Wilson, L. (1995). Explosive volcanic eruptions—IX: The transition between Hawaiian-style lava fountaining and Strombolian explosive activity. *Geophysical Journal International*, *121*(1), 226–232. https://doi.org/10.1111/j.1365-246X.1995.tb03523.x

Qiao, L., Head, J. W., Wilson, L., & Ling, Z. (2018). Lunar irregular Mare patch (IMP) sub-types: Linking their origin through hybrid relationships displayed at Cauchy 5 small shield volcano. Lunar and Planetary Science XLIX, Abstract 1390.

Qiao, L., Head, J. W., Wilson, L., Xiao, L., Kreslavsky, M., & Dufek, J. (2017). Ina pit crater on the Moon: Extrusion of waning-stage lava lake magmatic foam results in extremely young crater retention ages. *Geology*, *45*(5), 455–458. https://doi.org/10.1130/G38594.1

Renggli, C. J., King, P. L., Henley, R. W., & Norman, M. D. (2017). Volcanic gas composition, metal dispersion and deposition during explosive volcanic eruptions on the Moon. *Geochimica et Cosmochimica Acta*, *206*, 296–311. https://doi.org/10.1016/j.gca.2017.03.012

Rutherford, M. J., Head, J. W., Saal, A. E., Hauri, E., & Wilson, L. (2017). Model for the origin, ascent and eruption of lunar picritic magmas. *American Mineralogist*, *102*, 2045–2053. https://doi.org/10.2138/am-2017-5994ccbyncnd

Saal, A. E., Chaussidon, M., Gurenko, A. A., & Rutherford, M. (2018). Boron and Lithium contents and isotopic composition of the lunar volcanic glasses. 49th Lunar and Planetary Science Conference, Abstract 2575.

Schultz, P. H. (1976). *Moon morphology: Interpretations based on Lunar Orbiter Photography* (p. 626). Austin: University of Texas Press.

Self, S., Thordarson, T., Keszthelyi, L., Walker, G. P. L., Hon, K., Muphy, M. T., et al. (1996). A new model for the emplacement of Columbia River basalts as large, inflated pahoehoelava fields. *Geophysical Research Letters*, *23*(19), 2689–2692. https://doi.org/10.1029/96GL02450

Shearer, C. K., Hess, P. C., Wieczorek, M. A., Pritchard, M. E., Parmentier, E. M., Borg, L. E., et al. (2006). Thermal and magmatic evolution of the Moon. *Reviews in Mineralogy and Geochemistry*, *60*(1), 365–518. https://doi.org/10.2138/rmg.2006.60.4

Solomon, S. C., & Head, J. W. (1980). Lunar mascon basins: Lava filling, tectonics, and evolution of the lithosphere. *Reviews of Geophysics and Space Physics*, *18*(1), 107–141. https://doi.org/10.1029/RG018i001p00107

Wieczorek, M. A., Neumann, G. A., Nimmo, F., Kiefer, W. S., Taylor, G. J., Melosh, H. J., et al. (2013). The crust of the Moon as seen on GRAIL. *Science*, *339*(6120), 671–675. https://doi.org/10.1126/science.1231530

Wilhelms, D. E. (1987). The geologic history of the Moon. *U.S. Geological Survey Professional Paper*, *1348*, 302.

Wilson, L., Hawke, B. R., Giguere, T. A., & Petrycki, E. R. (2011). An igneous origin for Rima Hyginus and Hyginus Crater on the Moon. *Icarus*, *215*(2), 584–595. https://doi.org/10.1016/j.icarus.2011.07.003

Wilson, L., & Head, J. W. (1981). Ascent and eruption of basaltic magma on the Earth and Moon. *Journal of Geophysical Research*, *86*(B4), 2971–3001. https://doi.org/10.1029/JB086iB04p02971

Wilson, L., & Head, J. W. (2001). Lava fountains from the 1999 Tvashtar Catena fissure eruption on Io: Implications for dike emplacement mechanisms, eruption rates and crustal structure. *Journal of Geophysical Research*, *106*(E12), 32,997–33,004. https://doi.org/10.1029/2000JE001323

Wilson, L., & Head, J. W. (2003). Deep generation of magmatic gas on the Moon and implications for pyroclastic eruptions. *Geophysical Research Letters*, *30*(12), 1605. https://doi.org/10.1029/2002GL016082

Wilson, L., & Head, J. W. (2017a). Generation, ascent and eruption of magma on the Moon: New insights into source depths, magma supply, intrusions and effusive/explosive eruptions (Part 1: Theory). *Icarus*, *283*, 146–175. https://doi.org/10.1016/j.icarus.2015.12.039

Wilson, L., & Head, J. W. (2017b). Eruption of magmatic foams on the Moon: Formation in the waning stages of dike emplacement events as an explanation of "irregular mare patches". *Journal of Volcanology and Geothermal Research*, *335*, 113–127. https://doi.org/10.1016/j.volgeores.2017.02.009

Wilson, L., & Head, J. W. (2018). Lunar floor-fractured craters: Modes of dike and sill emplacement and implications of gas produciton and intrusion cooling on surface morphology and structure. *Icarus*, *305*, 105–122. https://doi.org/10.1016/j.icarus.2017.12.030

Zhang, F., Head, J. W., Basilevsky, A. T., Bugiolacchi, R., Komatsu, G., Wilson, L., et al. (2017). Newly-discovered ring-moat dome structures in the lunar maria: possible origins and implications. *Geophysical Research Letters*, *44*, 9216–9224. https://doi.org/10.1002/2017GL074416